1. Introduction

Lung cancer is the leading cause of cancer-related death in the United States [1] and throughout the world. Lung cancer is pathologically and clinically categorized into small cell lung cancer (SCLC) and non-small cell lung cancer (NSCLC). At the time of diagnosis most patients with NSCLC have inoperable disease with locally advanced or metastatic lesions, and chemotherapy with cytotoxic agents in such patients remains marginally effective [2,3]. With recent advances in molecular research, molecular-targeted agents such as gefitinib (IRESSA; AstraZeneca), an epidermal growth factor receptor (EGFR)-tyrosine kinase inhibitor (TKI), have emerged for the treatment of advanced NSCLC [4]. Previous studies have revealed that a high response rate to gefitinib was observed more frequently in females, never-smokers, Japanese patients, and patients with adenocarcinoma [5,6]. Recently, *EGFR* mutations in the TK domain have been identified in NSCLC [7] and have been associated with increased sensitivity to gefitinib in both retrospective [8–10] and prospective studies [11–15]. However, the therapeutic effect of gefitinib is not confined to patients whose tumors harbor *EGFR* mutations and other predictors of the efficacy of this agent are being investigated.

Increased uptake of ^{18}F-fluorodeoxyglucose (FDG) measured by positron emission tomography (PET) reflects glucose metabolism and proliferative activity of tumor cells [16,17]. Metabolic imaging with FDG-PET has widely been used for staging, restaging, and evaluating treatment efficacy in various cancers including NSCLC [18,19]. Several studies have indicated that FDG-PET is useful for the early evaluation of tumor response to anticancer drugs [20]. However, the clinical usefulness of FDG-PET as a predictor of treatment efficacy with gefitinib has not been evaluated. In the present study, we have attempted to assess the clinical value of FDG-PET for the early prediction of tumor response to gefitinib. Changes in the FDG uptake immediately after the initiation of therapy were compared with long-term efficacy of gefitinib in patients with advanced NSCLC.

2. Methods

2.1. Patients

From March 2005 to February 2007, five patients were enrolled in the present study (Table 1). The eligibility criteria were as follows: histologically or cytologically proven NSCLC; unresectable stage III/VI disease or recurrent disease after surgery; age over 20 years; measurable disease; Eastern Cooperative Oncology Group (ECOG) performance status 0–2; adequate bone marrow function, liver function, and renal function. Patients were excluded if they had interstitial pneumonitis or lung fibrosis identified by a chest X-ray or chest CT scan, diabetes mellitus, a concomitant serious illness, such as uncontrolled angina pectoris, myocardial infarction, heart failure, uncontrolled hypertension, infection, or pregnancy. The study protocol was approved by the institutional review board in Gunma University Hospital, and all patients gave their written informed consent. Genomic DNA was extracted from tumor samples and *EGFR* mutations in exons 19 and 21 were analyzed as described previously [13,21].

2.2. Assessment of tumor response by CT and FDG-PET

Within 14 days prior to the treatment, CT of the chest and abdomen, magnetic resonance imaging (MRI) of the whole brain, radionuclide bone scan, and FDG-PET were performed for pretreatment assessments. Patients received gefitinib 250 mg orally, once daily. Radiographic tumor response was evaluated according to the Response Evaluation Criteria in Solid Tumors (RECIST) [22], and assessments were performed every 4 weeks, then every 8 weeks following the fourth month. During the study and for 30 days after the last dose of gefitinib, patients were monitored for adverse events, which were graded according to the National Cancer Institute Common Toxicity Criteria (http://ctep.cancer.gov/reporting/ctc_v30.html).

On day 2 and at 4 weeks following the initiation of gefitinib, patients underwent FDG-PET to determine changes in the FDG uptake in the lesion. FDG was produced in the cyclotron facility of our institute [23] and PET was performed as described previously [24]. The patients fasted for at least 6 h before the PET studies. PET was performed using a whole-body PET scanner (SET 2400 W; Shimadzu, Kyoto, Japan) with 59.5 cm transverse fields of view and 20 cm axial field of view, which produced 63 image planes. Transverse resolution at the center of the field of view was 4.2 mm, full width, half maximum.

Imaging was initiated 50 min after the injection of 5–6 MBq/kg of ^{18}F-FDG. Two-dimensional data acquisition was performed by the simultaneous emission-transmission method with a rotating external source for 4–10 bed positions (8 min acquisition per bed position) according to the range of imaging. Attenuation-corrected images were reconstructed with the ordered-subsets expectation maximization algorithm into 128×128 matrices with pixel dimensions of 4.0 mm in plane and 3.125 mm axially. Coronal images with a 9.8 mm thickness were also reconstructed for visual interpretation. FDG uptake was evaluated as the maximal standardized uptake value (SUVmax) of the target lesions, which were assessable by CT. Changes in the FDG uptake was determined by the ratio of the SUVmax after gefitinib treatment to the SUVmax before the treatment (SUVmax%).

2.3. Statistical analysis

Progression-free survival (PFS) was defined as the interval between the date of gefitinib initiation and the date of the first observation of disease progression, or death from any cause. Patients who were alive without disease progression at the data cutoff point (the end of March 2007) were censored at the last point at which they were assessed to be progression-free.

3. Results

Characteristics of patients are shown in Table 1. In the present study, we could have five patients who were eligible

Table 1 Patient characteristics

Patient no.	Age	Gender	Smoking status[a]	Histology	Stage	[b]*EGFR* mutation	[c]CT response	PFS (M)	[d]OS (M)
1	56	F	0	Ad	IIIB	delE746-A750	PR	14.9	19.7
2	56	F	35	Ad	IV	delL747-P753	PR	4.5	6.3
3	80	F	0	Ad	IIIB	L858R	SD	12.9	16.9
4	59	F	0	Ad	IV	L858R	SD	12.5	21.0
5	78	F	40	Sq	IV	None	PD	ND	2.7

F: Female; Ad: adenocarcinoma; Sq: squamous cell carcinoma; PFS: progression-free survival; OS: overall survival; ND: not determined.
[a] Pack years.
[b] *EGFR* mutations in exon 19 or 21.
[c] CT response was evaluated according to the RECIST criteria.
[d] Patients 2–4 had died while Patients 1 and 5 were alive at the data cutoff point (end of March 2007).

for the present study and provided consents for participation. *EGFR* mutations were detected in tumor samples from four patients (Patients 1–4; Table 1). Patient 1 had received surgery, Patients 2 and 5 received systemic chemotherapy prior to gefitinib treatment, and Patients 3 and 4 were chemotherapy-naïve. Radiographic response to gefitinib therapy was as follows: two patients exhibited a partial response (PR), two patients had stable disease (SD) with a minor response (decreased tumor size, but not reaching criteria for PR), and one patient had progressive disease (PD). At the data cutoff point (median follow-up time of 16.9 months), all four patients who had responded to gefitinib had relapsed, and three patients had died (Table 1). The two patients with a best response to gefitinib of SD (Patients 3 and 4) had a PFS of >12 months; and thus obtained relatively long-term PFS despite having experienced only a minor response by RECIST criteria.

Within 2 days of starting gefitinib, FDG uptake had decreased from baseline by a mean (±standard deviation) SUVmax% of 61 ± 18 and 59 ± 12% in patients who had a PR (Patients 1 and 2) and those with SD (Patients 3 and 4), respectively (Table 2). Of note, tumor response was monitored by both CT and FDG-PET at 2 days after gefitinib initiation in a patient who experienced a PR (Patient 2), and the reduction in FDG uptake was detected earlier than the morphological change as detected by CT (Fig. 1). In the two patients with SD, decreased FDG uptake was also noted at 2 days after initiation of therapy (Fig. 2). In contrast, in the patient with PD, SUVmax% had increased from baseline (13 days prior to the treatment) by 153 ± 21% at 2 days after the initiation of gefitinib and increased further thereafter (Patient 5; Fig. 3).

At 4 weeks after the initiation of treatment, patients who had a PR or SD as best response to gefitinib experienced further decreases in mean SUVmax% by 26 ± 6 and 43 ± 10%, respectively (Table 2): SUVmax% was lower among patients with PR than those with SD (Table 2). In the patients who had PD, SUVmax% further increased by 232 ± 73% at 4 weeks after the initiation of therapy (Table 2). Thus, the tumor response as evaluated by FDG-PET (metabolic response) was correlated to the CT response, but could be detected earlier than by conventional CT.

4. Discussion

This is the first study to evaluate the clinical usefulness of FDG-PET for early prediction of the efficacy of gefitinib for the treatment of advanced NSCLC. In patients who experienced a tumor response (as measured by RECIST) with gefitinib, FDG uptake decreased within 2 days of gefitinib initiation, the decrease being more prominent at 4 weeks. In contrast, FDG uptake gradually increased >2-fold in patients who were non-responders to gefitinib. Interestingly, a marked decrease in FDG uptake was also observed in patients with SD who exhibited only a minor response on CT but had long-term PFS (12.9 and 12.5 months). In larger clinical trials of gefitinib monotherapy, symptom improvement was noted in more than 50% of patients with SD, which may contribute to an improvement of survival [5,6]. Recently, Hotta et al. reported that the overall survival in patients achieving SD with gefitinib treatment was significantly longer than in patients with PD [25]. Furthermore, previous studies have demonstrated that a decreased FDG uptake was a better predictor of PFS and overall survival than CT response to chemotherapy and chemoradiotherapy in patients with NSCLC [26–28]. Therefore, FDG-PET may be useful to predict better survival in patients who do not exhibit response by the RECIST criteria

Table 2 Changes in FDG uptake in target lesions before and after gefitinib treatment

Patient no.	Target lesion	[a]SUVmax (%)		
		Before	2 days	4 weeks
1	Primary	5.18	2.49(48)	1.23(24)
2a	Primary	9.59	8.31(87)	2.74(29)
2b	Adrenal	9.64	5.59(58)	3.12(32)
2c	Bone	9.50	4.61(49)	1.70(18)
3a	Primary	3.22	1.87(58)	1.62(50)
3b	Dissemi	3.16	1.92(61)	1.00[b](32)
4a	Primary	5.13	2.42(47)	1.65(32)
4b	Bone1	5.77	4.53(79)	3.19(55)
4c	Bone2	6.45	3.31(51)	2.81(44)
5a	Primary	3.77	6.68(177)	7.31(194)
5b	Lymph1	3.24	4.63(143)	10.27(317)
5c	Lymph2	5.59	7.69(138)	10.42(186)

[a] SUVmax% was defined as the ratio of the SUV max level at 2 days or 4 weeks after treatment to the level before treatment.
[b] If FDG uptake was not detected, the value of SUVmax was determined as 1.00.

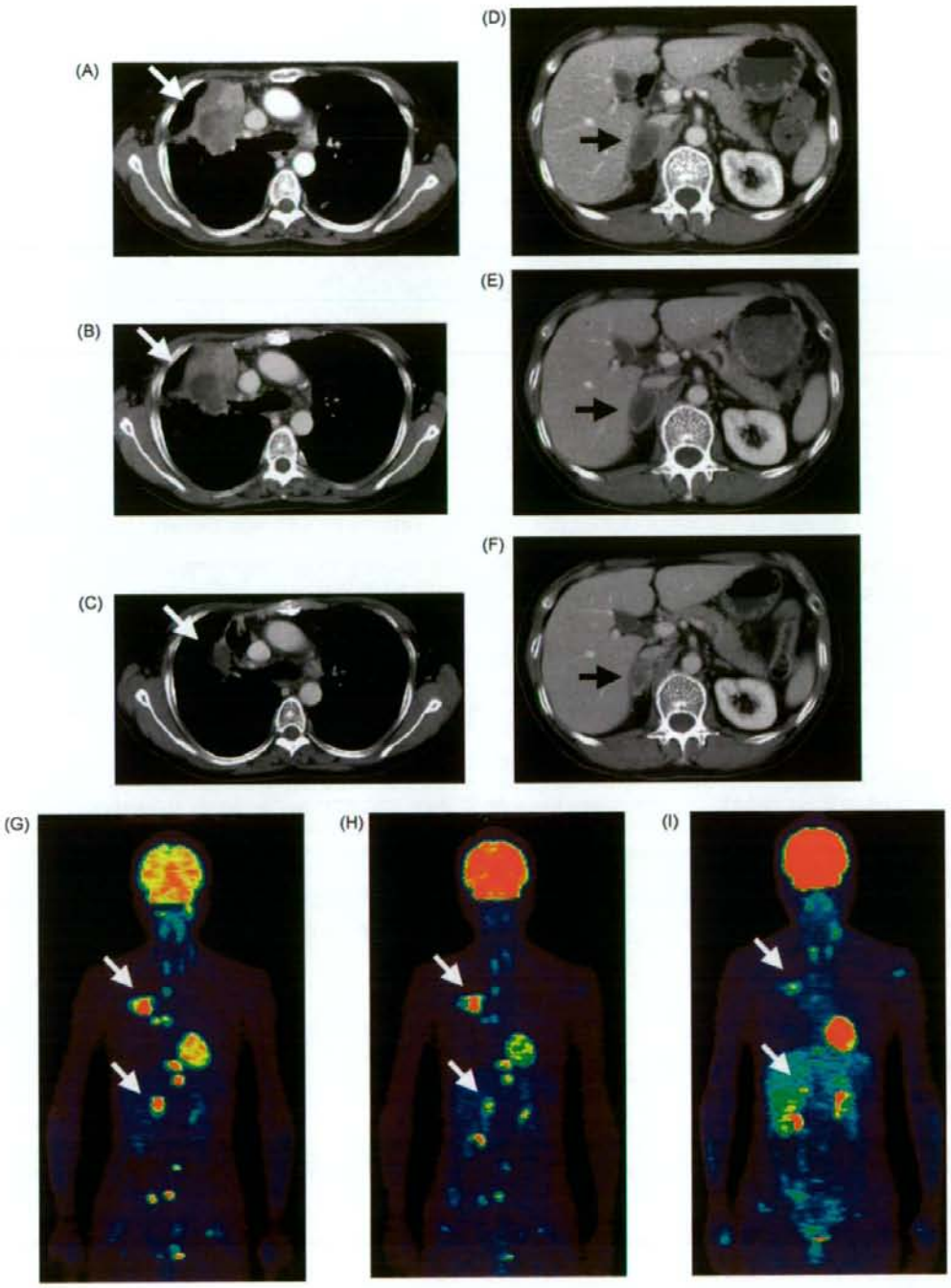

Fig. 1 A representative case (Patient 2) who exhibited PR according to the RECIST criteria. White arrows indicate the primary lesion as shown on CT before (A), and after 2 days (B) and 4 weeks (C) of the initiation of gefitinib. Black arrows indicate the metastatic adrenal lesion as shown on CT before (D), at 2 days (E) and 4 weeks (F). FDG uptake as measured by PET before (G), at 2 days (H) and 4 weeks (I). Upper arrows indicate the primary lesion and lower arrows indicate the adrenal lesion.

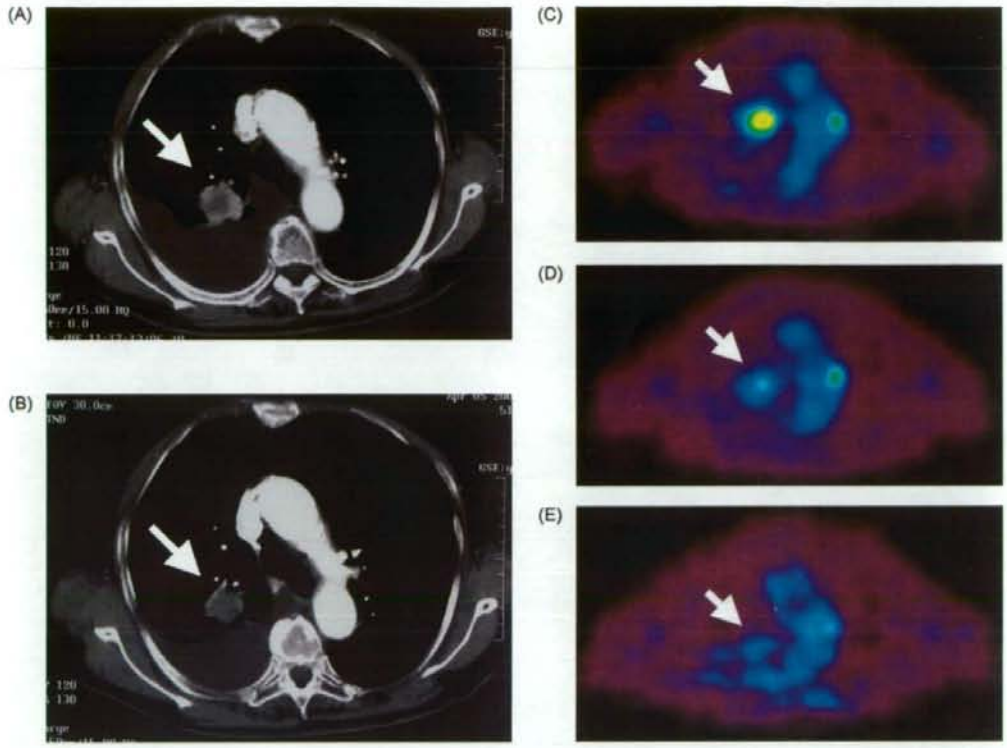

Fig. 2 A representative case (Patient 3) who had SD (with minor response) according to the RECIST criteria but achieved metabolic response as evaluated by FDG-PET. The tumor in the right upper lobe (A, arrow) shows no shrinkage on CT after 4 weeks (B) of the initiation of gefitinib. FDG-PET shows intense uptake (arrow) before the therapy on CT (C), but the uptake has gradually decreased on 2 days (D), and 4 weeks (E) of the initiation of gefitinib.

but who remain progression free for long periods (e.g., 12 months).

Tumor response to anticancer drugs is generally evaluated by the change in tumor size before and after the treatment using morphological images generated by X-ray and/or CT. However, these morphology-based responses may take several weeks to occur. In addition, changes in size do not always reflect the changes in viable tumor cells since tumors usually contain necrotic and fibrotic tissues and conventional morphological imaging cannot distinguish cancer cells from these coexisting non-cancerous tissues. Compared with morphological images, FDG-PET has the advantage of being able to assess viable tumor cells, in which FDG preferentially accumulates in accordance with the activity of glucose transporters and phosphorylation, but not in fibrotic or necrotic tissues. Thus, evaluating efficacy of anticancer drugs based on the metabolic response with FDG-PET appears to be more sensitive and might detect the tumor response earlier than that with conventional CT. In this study, we could detect the reduction in FDG uptake earlier than the morphological change at 2 days of gefitinib initiation in a patient with PR (Fig. 1). On the other hand, we could not correlate changes in the size of the tumor with the increased FDG uptake in a patient with PD, since CT was not performed at 2 days after the initiation of gefitinib in this case. It is not likely that CT could detect enlargement of the tumor at 2 days of treatment initiation in the PD case. Remarkable increase in the FDG uptake itself would also be elucidated. Further study is needed to determine the correlative change in the size and glucose metabolism in case with PD after gefitinib therapy.

A number of studies have indicated the usefulness of FDG-PET for early evaluation of tumor response to anticancer drugs [20]. Recently, it has been reported that FDG-PET could predict response to imatinib mesylate early in the course of treatment for gastrointestinal stromal tumors [29–31]. As for the molecular-targeted agents, gefitinib was the first drug that has been approved for the treatment of patients with advanced, chemotherapy-refractory NSCLC [4]. *EGFR* mutations in the TK domain of the receptor are now believed to be an important predictor of response to gefitinib therapy. However, several recent studies have reported that positive predictive value of *EGFR* mutations for response to TKI inhibitors has varied widely [32] and it was as low as 16% [33], indicating that the accurate evaluation of the *EGFR* mutations still needs to be standardized. In addition, the benefits of gefitinib treatment are not limited to patients whose tumors have the *EGFR* mutations; the retrospective studies showed that 23% of the EGFR TKI-responsive tumors do not harbor the *EGFR* mutations [32].

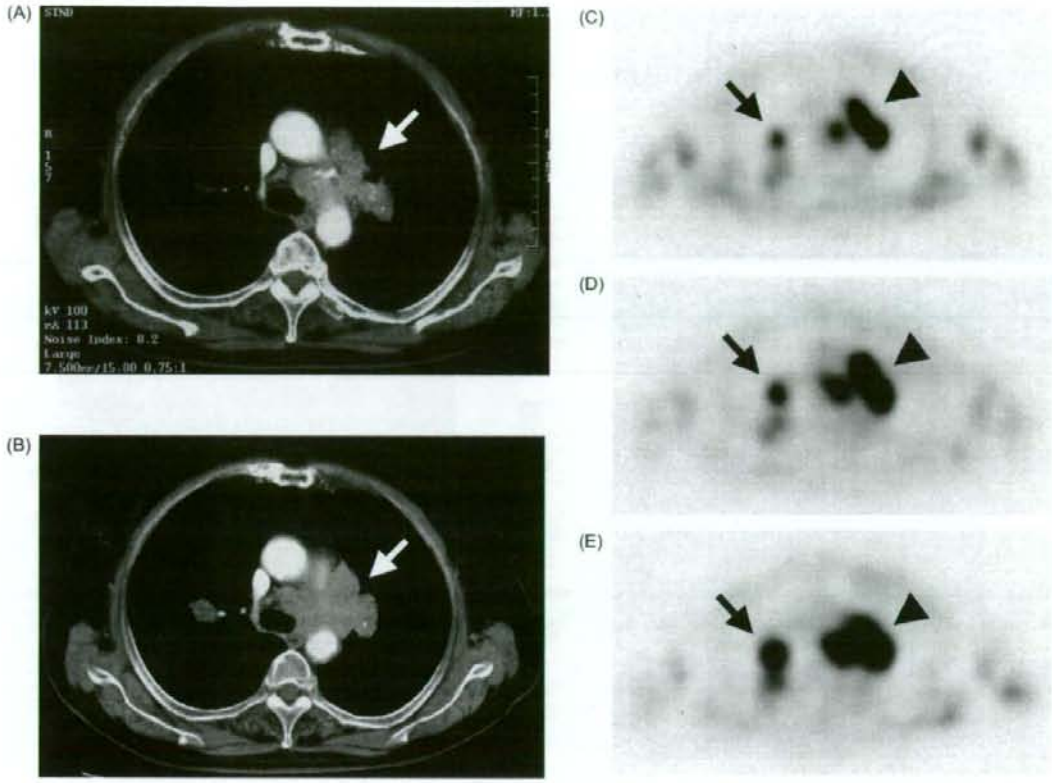

Fig. 3 A representative case (Patient 5) who did not respond to gefitinib. White arrows indicate the metastatic lymph nodes as shown on CT before (A) and 4 weeks after the initiation of gefitinib (B). PET shows that the uptake of FDG in the primary lesion (arrow) and the metastatic lymph nodes (arrowheads) before the therapy (C) has increased after 2 days (D) and 4 weeks (E) of the initiation of gefitinib.

A retrospective analysis of the IDEAL trials revealed that *EGFR* mutation-positive patients did not have better overall survival than those without the mutations [34]. Therefore, alternative approaches for identifying which NSCLC patients will benefit from gefitinib therapy are required. Of note, Su et al. demonstrated dramatic decreases in tumor FDG uptake in mice xenografts of gefitinib-sensitive NSCLC cell lines 2 days after treatment [35]. They also demonstrated that the treatment with gefitinib led to the decrease in FDG uptake in gefitinib-sensitive NSCLC cells as early as 2 h before changes in cellular proliferation and apoptosis [35]. Interestingly, in parallel to the decrease in FDG uptake, the gefitinib treatment for 2 h reduced the level of GLUT3 transporter in the plasma membrane fraction, but increased the level in the cytosol fraction [35]. Thus, one possible mechanism behind the early reduction of the FDG uptake by gefitinib is that gefitinib causes the glucose transporter to translocate from the plasma membrane to the cytosol in gefitinib-sensitive cancer cells followed by the changes in cellular proliferation and apoptosis. Further studies are needed to elucidate how TKI inhibitors lead to the translocation of glucose transporter and the resultant decrease in FDG uptake in gefitinib-sensitive cells. Nevertheless, our preliminary results are in agreement with their observation in mice, suggesting the potential use of FDG-PET for the early prediction of the efficacy of gefitinib in patients with NSCLC.

Interstitial lung disease (ILD) is a serious adverse event that has been associated with the administration of gefitinib. Ando et al. reported that 3.5% of the patients with NSCLC who had received gefitinib developed ILD and 1.6% of them died [36]; the median duration from the gefitinib initiation to the development of ILD was 31 days (interquartile range of 18–50 days). If lack of response to gefitinib could be predicted early in the course of treatment, treatment could be stopped/switched thus, avoiding the development of unnecessary toxicities as well as saving costs for the treatment thereafter.

In summary, our preliminary results suggest the potential use of FDG-PET for the early prediction of gefitinib efficacy for the treatment of NSCLC. The response to gefitinib may be predicted as early as 2 days after initiation of the treatment that is consistent with the observations of animal study with mice by Su et al. [35]. Since the number of patients enrolled in this study was small, further larger prospective studies are needed to confirm the usefulness of FDG-PET.

Conflict of interest

All authors have no financial or personal relationships with other people or organizations that could inappropriately influence our work.

Acknowledgment

This work was supported in part by Grant 18790532 (to N.S.) from the Ministry of Education, Culture, Sports, Science and Technology, Japan.

References

[1] Jemal A, Siegel R, Ward E, Murray T, Xu J, Thun MJ. Cancer statistics, 2007. CA Cancer J Clin 2007;57:43–66.

[2] Chemotherapy in non-small cell lung cancer: a meta-analysis using updated data on individual patients from 52 randomised clinical trials. Non-small Cell Lung Cancer Collaborative Group. BMJ 1995;311:899–909.

[3] Breathnach OS, Freidlin B, Conley B, Green MR, Johnson DH, Gandara DR, et al. Twenty-two years of phase III trials for patients with advanced non-small-cell lung cancer: sobering results. J Clin Oncol 2001;19:1734–42.

[4] Pao W, Miller VA. Epidermal growth factor receptor mutations, small-molecule kinase inhibitors, and non-small-cell lung cancer: current knowledge and future directions. J Clin Oncol 2005;23:2556–68.

[5] Fukuoka M, Yano S, Giaccone G, Tamura T, Nakagawa K, Douillard JY, et al. Multi-institutional randomized phase II trial of gefitinib for previously treated patients with advanced non-small-cell lung cancer (The IDEAL 1 Trial) [corrected]. J Clin Oncol 2003;21:2237–46.

[6] Kris MG, Natale RB, Herbst RS, Lynch Jr TJ, Prager D, Belani CP, et al. Efficacy of gefitinib, an inhibitor of the epidermal growth factor receptor tyrosine kinase, in symptomatic patients with non-small cell lung cancer: a randomized trial. JAMA 2003;290:2149–58.

[7] Shigematsu H, Gazdar AF. Somatic mutations of epidermal growth factor receptor signaling pathway in lung cancers. Int J Cancer 2006;118:257–62.

[8] Lynch TJ, Bell DW, Sordella R, Gurubhagavatula S, Okimoto RA, Brannigan BW, et al. Activating mutations in the epidermal growth factor receptor underlying responsiveness of non-small-cell lung cancer to gefitinib. N Engl J Med 2004;350:2129–39.

[9] Paez JG, Janne PA, Lee JC, Tracy S, Greulich H, Gabriel S, et al. EGFR mutations in lung cancer: correlation with clinical response to gefitinib therapy. Science 2004;304:1497–500.

[10] Pao W, Miller V, Zakowski M, Doherty J, Politi K, Sarkaria I, et al. EGF receptor gene mutations are common in lung cancers from "never smokers" and are associated with sensitivity of tumors to gefitinib and erlotinib. Proc Natl Acad Sci USA 2004;101:13306–11.

[11] Asahina H, Yamazaki K, Kinoshita I, Sukoh N, Harada M, Yokouchi H, et al. A phase II trial of gefitinib as first-line therapy for advanced non-small cell lung cancer with epidermal growth factor receptor mutations. Br J Cancer 2006;95:998–1004.

[12] Inoue A, Suzuki T, Fukuhara T, Maemondo M, Kimura Y, Morikawa N, et al. Prospective phase II study of gefitinib for chemotherapy-naive patients with advanced non-small-cell lung cancer with epidermal growth factor receptor gene mutations. J Clin Oncol 2006;24:3340–6.

[13] Sunaga N, Tomizawa Y, Yanagitani N, Iijima H, Kaira K, Shimizu K, et al. Phase II prospective study of the efficacy of gefitinib for the treatment of stage III/IV non-small cell lung cancer with EGFR mutations, irrespective of previous chemotherapy. Lung Cancer 2007;56:383–9.

[14] Sutani A, Nagai Y, Udagawa K, Uchida Y, Koyama N, Murayama Y, et al. Gefitinib for non-small-cell lung cancer patients with epidermal growth factor receptor gene mutations screened by peptide nucleic acid-locked nucleic acid PCR clamp. Br J Cancer 2006;95:1483–9.

[15] Yoshida K, Yatabe Y, Park JY, Shimizu J, Horio Y, Matsuo K, et al. Prospective validation for prediction of gefitinib sensitivity by epidermal growth factor receptor gene mutation in patients with non-small cell lung cancer. J Thorac Oncol 2007;2:22–8.

[16] Minn H, Joensuu H, Ahonen A, Klemi P. Fluorodeoxyglucose imaging: a method to assess the proliferative activity of human cancer in vivo. Comparison with DNA flow cytometry in head and neck tumors. Cancer 1988;61:1776–81.

[17] Vesselle H, Schmidt RA, Pugsley JM, Li M, Kohlmyer SG, Vallires E, et al. Lung cancer proliferation correlates with [F-18]fluorodeoxyglucose uptake by positron emission tomography. Clin Cancer Res 2000;6:3837–44.

[18] Oriuchi N, Higuchi T, Ishikita T, Miyakubo M, Hanaoka H, Iida Y, et al. Present role and future prospects of positron emission tomography in clinical oncology. Cancer Sci 2006;97:1291–7.

[19] Rohren EM, Turkington TG, Coleman RE. Clinical applications of PET in oncology. Radiology 2004;231:305–32.

[20] Young H, Baum R, Cremerius U, Herholz K, Hoekstra O, Lammertsma AA, et al. Measurement of clinical and subclinical tumour response using [^{18}F]-fluorodeoxyglucose and positron emission tomography: review and 1999 EORTC recommendations. European Organization for Research and Treatment of Cancer (EORTC) PET Study Group. Eur J Cancer 1999;35:1773–82.

[21] Tomizawa Y, Iijima H, Sunaga N, Sato K, Takise A, Otani Y, et al. Clinicopathologic significance of the mutations of the epidermal growth factor receptor gene in patients with non-small cell lung cancer. Clin Cancer Res 2005;11:6816–22.

[22] Therasse P, Arbuck SG, Eisenhauer EA, Wanders J, Kaplan RS, Rubinstein L, et al. New guidelines to evaluate the response to treatment in solid tumors. European Organization for Research and Treatment of Cancer, National Cancer Institute of the United States, National Cancer Institute of Canada. J Natl Cancer Inst 2000;92:205–16.

[23] Oriuchi N, Tomiyoshi K, Inoue T, Ahmad K, Sarwar M, Tokunaga M, et al. Independent thallium-201 accumulation and fluorine-18-fluorodeoxyglucose metabolism in glioma. J Nucl Med 1996;37:457–62.

[24] Kaira K, Oriuchi N, Otani Y, Yanagitani N, Sunaga N, Hisada T, et al. Diagnostic usefulness of fluorine-18-{alpha}-methyltyrosine positron emission tomography in combination with ^{18}F-fluorodeoxyglucose in sarcoidosis patients. Chest 2007;131:1019–27.

[25] Hotta K, Matsuo K, Ueoka H, Kiura K, Tabata M, Harita S, et al. Continued gefitinib treatment after disease stabilisation prolongs survival of Japanese patients with non-small-cell lung cancer. Okayama Lung Cancer Study Group experience. Ann Oncol 2005;16:1817–23.

[26] Hoekstra CJ, Stroobants SG, Smit EF, Vansteenkiste J, van Tinteren H, Postmus PE, et al. Prognostic relevance of response evaluation using [^{18}F]-2-fluoro-2-deoxy-D-glucose positron emission tomography in patients with locally advanced non-small-cell lung cancer. J Clin Oncol 2005;23:8362–70.

[27] Mac Manus MP, Hicks RJ, Matthews JP, McKenzie A, Rischin D, Salminen EK, et al. Positron emission tomography is superior to computed tomography scanning for response-assessment after radical radiotherapy or chemoradiotherapy in patients with non-small-cell lung cancer. J Clin Oncol 2003;21:1285–92.

[28] Weber WA, Petersen V, Schmidt B, Tyndale-Hines L, Link T, Peschel C, et al. Positron emission tomography in non-small-cell lung cancer: prediction of response to chemotherapy

by quantitative assessment of glucose use. J Clin Oncol 2003;21:2651–7.

[29] Demetri GD, von Mehren M, Blanke CD, Van den Abbeele AD, Eisenberg B, Roberts PJ, et al. Efficacy and safety of imatinib mesylate in advanced gastrointestinal stromal tumors. N Engl J Med 2002;347:472–80.

[30] Gayed I, Vu T, Iyer R, Johnson M, Macapinlac H, Swanston N, et al. The role of ^{18}F-FDG PET in staging and early prediction of response to therapy of recurrent gastrointestinal stromal tumors. J Nucl Med 2004;45:17–21.

[31] Stroobants S, Goeminne J, Seegers M, Dimitrijevic S, Dupont P, Nuyts J, et al. ^{18}FDG-positron emission tomography for the early prediction of response in advanced soft tissue sarcoma treated with imatinib mesylate (Glivec). Eur J Cancer 2003;39:2012–20.

[32] Sequist LV, Bell DW, Lynch TJ, Haber DA. Molecular predictors of response to epidermal growth factor receptor antagonists in non-small-cell lung cancer. J Clin Oncol 2007;25:587–95.

[33] Tsao MS, Sakurada A, Cutz JC, Zhu CQ, Kamel-Reid S, Squire J, et al. Erlotinib in lung cancer—molecular and clinical predictors of outcome. N Engl J Med 2005;353:133–44.

[34] Bell DW, Lynch TJ, Haserlat SM, Harris PL, Okimoto RA, Brannigan BW, et al. Epidermal growth factor receptor mutations and gene amplification in non-small-cell lung cancer: molecular analysis of the IDEAL/INTACT gefitinib trials. J Clin Oncol 2005;23:8081–92.

[35] Su H, Bodenstein C, Dumont RA, Seimbille Y, Dubinett S, Phelps ME, et al. Monitoring tumor glucose utilization by positron emission tomography for the prediction of treatment response to epidermal growth factor receptor kinase inhibitors. Clin Cancer Res 2006;12:5659–67.

[36] Ando M, Okamoto I, Yamamoto N, Takeda K, Tamura K, Seto T, et al. Predictive factors for interstitial lung disease, antitumor response, and survival in non-small-cell lung cancer patients treated with gefitinib. J Clin Oncol 2006;24:2549–56.

Abdominal Imaging

Published online: 12 July 2007

Abdom Imaging (2008) 33:353–356
DOI: 10.1007/s00261-007-9252-y

Diffusion-weighted magnetic resonance imaging of the body in venous thrombosis: a report of four cases

Masumi Nakahashi,[1] Noriko Sato,[2] Yoshito Tsushima,[1] Makoto Amanuma,[1] Keigo Endo[1]

[1]Department of Diagnostic Radiology and Nuclear Medicine, Gunma University Graduate School of Medicine, Maebashi, Japan
[2]Department of Radiology, National Center Hospital for Mental, Nervous and Muscular Disorders, National Center of Neurology and Psychiatry, 4-1-1 Ogawahigashi-chyo, Kodaira, Tokyo, Japan

The diffusion-weighted (DW) sequence is frequently used in magnetic resonance imaging (MRI) to detect acute cerebral infarctions as well as various infectious and metabolic diseases. In addition, in cerebral venous thrombosis there have been reports of increased signal corresponding to the presence of intravascular clots [1–5]. However, the presence of such signals has not yet been evaluated in extra-cerebral venous thrombosis (VT).

Recent advances in imaging have enabled high-b-value-DW images of the body to be obtained [6–7]. Thus, in the present study we used DW imaging (DWI) to evaluate four cases of VT of the abdomen and leg and compared the findings with contrast-enhanced computed tomography (CT) images.

Case reports

Case 1

An 81-year-old woman was admitted to hospital 2 days after the sudden onset of severe pain and edema in her left lower leg. The patient had an 8-year history of acoustic neurinoma and normal pressure hydrocephalus. Because deep VT was suspected, CT examination with and without contrast material was performed. It showed swelling in the left lower leg with increasing density of the subcutaneous tissue. The superficial femoral and enlarged popliteal veins were shown as defects of enhancement inside the veins (Figs. 1A, B). Because CT was performed only on her leg, MRI was immediately performed just after CT, with lower abdominal and pelvic images obtained in addition to images of the leg. MRI was performed on a 1.0-T unit (Harmony; Siemens Medical Systems, Erlangen, Germany) equipped with a body array coil. The axial T1-weighted fast low angle shot gradient echo (FLASH) images and turbo spin echo T2-weighted imaging parameters were as follows: TR/TE, 195/7.49 and 4360/95; slice thickness, 8 mm; matrix, 288 × 384; field of view, 350 × 262 mm^2; and 1 average. A spin echo–echo planner imaging (SE-EPI) sequence with chemical shift selective (CHESS) pulse was used in DWI. The DWI parameters were as follows: TR/TE, 10000/86; b-factor = 0, 1,000; slice thickness, 4 mm; matrix, 128 × 75; field of view, 400 × 400 mm^2; and 8 averages. The scanning time of DWI was 5 min and 30 s. Diffusion weighted images were acquired with diffusion sensitization gradients applied in three orthogonal directions. After scanning, maximum intensity projection (MIP) images and coronal multiplanar reconstruction (MPR) images with a section thickness of 7 mm were produced. DWI demonstrated abnormally increased signal intensity along the left femoral and focally dilated popliteal vein (Fig. 1C). The ADC value of the thrombosis was 1.5×10^{-3} mm^2/s. There was no high-intensity lesion in the right lower leg nor in the inferior vena cave (IVC), which appeared as a flow-void in the other sequences. These CT and MRI findings indicated a diagnosis of VT of the left leg. Immediately heparin and warfarin anticoagulation was initiated.

Case 2

A 41-year-old woman with a history of repetitive colds noticed exacerbation of the cough and the appearance of chest pain, shortness of breath, lower leg fatigue and pain over the several months prior to admission. At hospital,

Correspondence to: Noriko Sato; *email:* satogunma@yahoo.co.jp

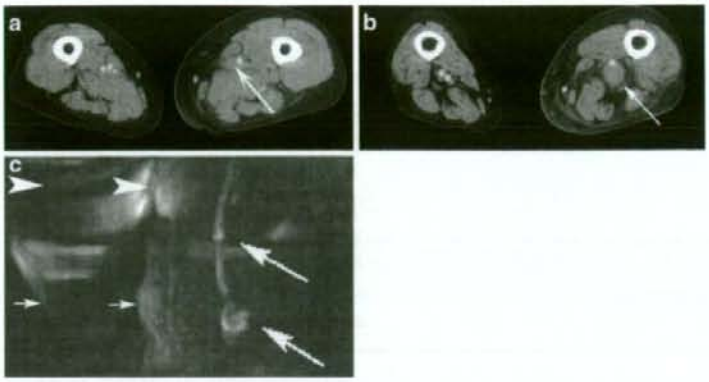

Fig. 1 Case 1. An 81-year-old woman with severe pain and edema in her left lower leg. **A** and **B** Axial enhanced CT image obtained 2 days after sudden onset shows swelling of the left leg, and that the superficial femoral (**A**) and focally dilated popliteal (**B**) veins are not enhanced, representing a venous thrombus (*arrow*). **C** Coronal oblique maximum intensity projection (*MIP*) image from DWI of the hip (*arrowhead*) and bilateral femurs (*small arrows*) shows luminal and nodular hyperintensity (*arrows*) in the left superficial femoral and focally dilated popliteal veins. The ADC value of the thrombus was 1.5×10^{-3} mm^2/s.

screening CT was performed, which showed calcification with a focal low density in the IVC. After injection of contrast material, a defect was detected in the IVC (Fig. 2A). On MRI, both T2-weighted and DWI showed an ill-defined luminal-shaped hyperintensity region, representing a thrombus in the IVC (Fig. 2B, C). DWI was performed from the level of the diaphragm to the iliac crest. Scanning time was 5 min and 30 s. The ADC value of the thrombosis was 1.6×10^{-3} mm^2/s. After diagnosis, anticoagulation therapy was performed in a hospital. One year later she was still under medication and follow-up CT, Doppler sonography and MRI studies, including MR venography, were performed. On CT examination, the thrombus was still in the IVC, localized at the renal hilar level, and collateral formation had developed along the IVC (Fig. 2D, E). Doppler sonography showed the existence of a VT. On MR venography of the IVC, the venous flow was unclear above the renal hilar level to the top of the IVC due to its slow flow. DWI no longer showed any high intensity area in the IVC (Fig. 2F). The ADC value of the region corresponding to the thrombus had slightly increased to 1.8×10^{-3} mm^2/s.

Case 3

A 57-year-old woman had a 16-year history of myotonic dystrophy, and then 5 years prior to admission she developed difficulty in walking. Follow-up MRI for assessment of the muscular system was performed. Coronal short TI inversion recovery (STIR) imaging and axial DWI of the lower extremity were performed. DWI above and under the knee was performed in sequence, taking 11 min in total. The STIR parameters were as follows: TR/TE/TI, 4210/85/150; slice thickness, 7 mm (10% gap); matrix, 512×216; field of view, 360×360 mm^2; and 2 averages. MRI showed her left leg was edematous, and on DWI there was a high signal spot in the medial side of the left leg. The ADC value could not be obtained because we used only one *b* factor (1,000) in this case. After repeated careful questioning, she reported that she had noticed edema in her lower leg about two weeks previously. Despite the lack of acute phenomena, there was slightly pain and swelling only on the left side. To confirm VT, CT with contrast material was performed two days later and revealed a defect of enhancement of the left fibular veins, which indicated VT. Anticoagulation therapy was then initiated.

Case 4

A 57-year-old man with a history of chronic myositis underwent MRI for follow-up assessment of the muscular system. DWI of the lower extremity was performed over 11 min. In the right lower leg, DWI showed areas of abnormally increased signal intensity, which were shown to correspond to varicose veins on coronal STIR images. The ADC value could not be obtained because we used only one *b* factor (1,000) in this case. CT was performed 3 days later and showed a VT inside the varicose veins. Anticoagulation therapy was then initiated.

Discussion

In all four cases of VT, DWI demonstrated abnormally increased signal intensity of intravenous clots, similar to previous findings for cerebral VT [1–5]. Venous thrombosis in extra-cerebral veins has not been previously demonstrated by DWI.

Venous thrombosis is a relatively common and potentially life-threatening condition, accounting for almost all instances of pulmonary embolism. Venous thrombosis has multiple causes, often related to varicose veins or stagnation of circulation that may occur during long flights or postoperative bed rest. In our study, patients 3 and 4 were suffering from myogenic disease and had already experienced difficulty walking for a few years. Thus, they had limited movement, a condition that tends to lead to the formation of thrombi. In patients 1

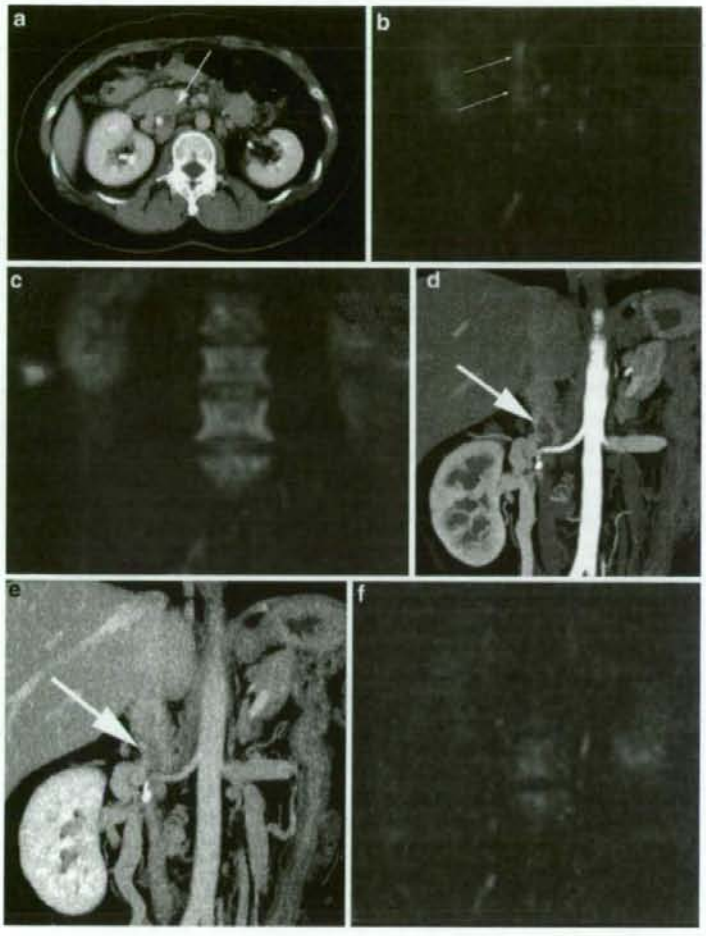

Fig. 2 Case 2. A 41-year-old woman with a history of repetitive colds. **A** Enhanced CT image shows a defect beside calcification in the IVC (*arrow*). **B** Coronal multiplanar reconstruction (*MPR*) image from DWI shows band-like hyperintensity (*arrows*) in the IVC at the renal hilar level. The ADC value of the thrombus was 1.6×10^{-3} mm^2/s. **C** Coronal MPR image from DWI, closer to the back. Vertebral bodies and both kidneys show as high signal intensity. **D** and **E** One year later, follow-up CT was performed, arterial (**D**) and venous (**E**) phase. Coronal reconstructed CT images indicate the defect beside calcification left in the IVC. **F** Follow-up DWI shows no hyperintensity lesion in the IVC. The ADC value of the region corresponding to the thrombus increased slightly to 1.8×10^{-3} mm^2/s.

and 2, a predisposing cause for their VT could not be found. Although the location of thrombi varies, they are frequently observed in the leg and pelvis [6]. In the present series, three patients had a thrombus in the leg, while the remaining patient had one in the IVC.

Diffusion weighted imaging provides information based on the molecular motion of water. Because it was previously difficult to use high *b*-values on DWI of the body, various truncal neoplasms were examined using low *b*-values, which are insufficient to observe molecular diffusion, to investigate their histopathologies [8]. Recently, a high *b*-value DW sequence was developed that allows examination of the whole body. Using a strong motion-probing gradient with high *b*-values not only provides information about molecular diffusion but also effectively suppresses blood flow signals. An increased DWI signal in vessels indicates the presence of intravascular clots, as confirmed by contrast-enhanced CT in the present study. A thrombus, which is viscous, is expected to show high signal intensity on DWI [9]. This is particularly true when a thrombus is imaged relatively quickly after onset, as in patients 1 (2 days) and 3 (2 weeks) in the present series. In patients 2 and 4, there were few subjective symptoms and the times of onset could not be established. However, we believe the follow-up MRI and CT studies in patient 2 indicated that the VT in the first study included a relatively young thrombosis in part, because the high signal on DWI disappeared on the follow-up MR study one year later. This phenomenon has been already shown in the head [1–5].

Diffusion weighted imaging does not require contrast media or exposure to radiation, therefore patients who have renal failure, an iodine allergy or the young could be safely examined to detect acute or subacute thrombosis. In the diagnosis of VT in the body, MR venography and Doppler sonography have also been universally used as noninvasive diagnostic clues. However, it is sometimes difficult to demonstrate the extent of

VT by MR venography because of the slow flow around the thrombosis. Doppler sonography is more accurate in demonstrating VT existence. However, DW images would also indicate the age of a thrombosis; this information cannot be obtained either by MR venography or Doppler sonography. This finding may be a diagnostic clue to the onset of VT and evidence of the need for medication. In addition, the ADC value would also be a marker of age. For example, in Patient 2 the ADC value of the thrombus was higher on follow-up DW images; it had increased from 1.6 to 1.8×10^{-3} mm^2/s. Previous reports have demonstrated that the ADC value of a malignant tumor in the liver is $0.8–1.7 \times 10^{-3}$ mm^2/s, while that of a benign tumor is $1.8–3.0 \times 10^{-3}$ mm^2/s [10–12]. The ADC values of the venous thrombi in the present study were between those of benign and malignant tumors. However, we examined only two cases; further examination is required.

In conclusion, DWI showed high signal intensity regions that represented thrombi in four cases of VT in the body and extremities. This finding may be a diagnostic clue to onset of VT and may provide evidence of the need for medication without contrast media or exposure to radiation.

References

1. Chang R, Friedman DP (2004) Isolated cortical venous thrombosis presenting as subarachnoid hemorrhage: a report of three cases. AJNR Am J Neuroradiol 25:1676–1679
2. Chuah KC, Stuckey SL, Berman IG (2004) Silent embolism in diagnostic cerebral angiography: detection with diffusion-weighted imaging. Austr Radiol 48:133–138
3. Corvol JC, Oppenheim C, Manai R (1998) Diffusion-weighted magnetic resonance imaging in a case of cerebral venous thrombosis. Stroke 29:2649–2652
4. Feiwell RJ, Besmertis L, Sarkar R, Saloner DA, Rapp JH (2001) Detection of clinically silent infarcts after carotid endarterectomy by use of diffusion-weighted imaging. AJNR Am J Neuroradiol 22:646–649
5. Sarma D, Farb RI, Mikulis DJ, terBrugge KG (2004) Reversal of restricted diffusion in cerebral venous thrombosis: case report. Neuroradiology 46:118–121
6. Spritzer CE, Arata MA, Freed KS (2001) Isolated pelvic deep venous thrombosis: relative frequency as detected with MR imaging. Radiology 219:521–525
7. Takahara T, Imai Y, Yamashita T, Yasuda S, Nasu S, Van Cauteren M (2004) Diffusion weighted whole body imaging with background body signal suppression (DWIBS): technical improvement using free breathing, STIR and high resolution 3D display. Radiat Med 22:275–282
8. Byun WM, Shin SO, Chang Y, Lee SJ, Finsterbusch J, Frahm J (2002) Diffusion-weighted MR imaging of metastatic disease of the spine: assessment of response to therapy. AJNR Am J Neuroradiol 23:906–912
9. Favrole P, Guichard JP, Crassard I (2004) Diffusion-weighted imaging of intravascular clots in cerebral venous thrombosis. Stroke 35:99–103
10. Ichikawa T, Haradome H, Hachiya J, et al. (1998) Diffusion-weighted MR imaging with a single-shot echoplanar sequence: detection and characterization of focal hepatic lesions. AJR Am J Roentgenol 170:397–402
11. Namimoto T, Yamashita Y, Sumi S, et al. (1997) Focal liver masses characterization with diffusion-weighted echo-planar MR imaging. Radiology 204:739–744
12. Kim T, Murakami T, Takahashi S, et al. (1999) Diffusion-weighted single-shot echoplanar MR imaging for liver disease. AJR Am J Roentgenol 173:393–398

Ann Nucl Med (2008) 22:395–401
DOI 10.1007/s12149-008-0128-1

ORIGINAL ARTICLE

Detection of metastatic lesions from malignant pheochromocytoma and paraganglioma with diffusion-weighted magnetic resonance imaging: comparison with ^{18}F-FDG positron emission tomography and ^{123}I-MIBG scintigraphy

Akie Takano · Noboru Oriuchi · Yoshito Tsushima · Ayako Taketomi-Takahashi · Takahito Nakajima · Yukiko Arisaka · Tetsuya Higuchi · Makoto Amanuma · Keigo Endo

Received: 29 November 2007 / Accepted: 15 January 2008

Abstract
Objective To investigate the diagnostic features of whole-body diffusion-weighted magnetic resonance imaging (DWI) as compared with 2-[^{18}F]-fluoro-2-deoxy-D-glucose positron emission tomography (FDG-PET) and ^{123}I-meta-iodo-benzyl guanidine scintigraphy (MIBG) on metastatic lesions of patients with malignant pheochromocytoma or paraganglioma.
Methods We prospectively studied 11 patients with histologically confirmed pheochromocytoma/paraganglioma and possible metastatic lesions. FDG-PET, MIBG, and DWI examinations were performed within 1 week, and the images were visually interpreted. Abnormal positive uptake either on MIBG or on FDG-PET was considered as metastases. Abnormal high signal intensities on DWI were considered as metastases using conventional T1- and T2-weighted images as reference.
Results FDG-PET and DWI demonstrated metastatic lesions in all 11 patients, but MIBG showed no metastatic lesions in two patients. The numbers of lymph node metastases depicted on FDG-PET, MIBG, and DWI were 19, 6, and 39; bone metastases were 50, 49, and 60; liver metastases were 9, 9, and 15; lung metastases were 5, 7, and 5, respectively. MIBG failed to demonstrate many metastatic lesions, which were demonstrated on FDG-PET or DWI, although two mediastinal lymph node metastases, three lung metastases, and six bone metastases, which were not seen on DWI, were clearly demonstrated on MIBG. DWI showed 15 liver metastases, but 6 of them were not seen on FDG-PET or MIBG.
Conclusions DWI may be particularly advantageous in depicting lymph node and liver metastases and may have a higher rate of detecting metastatic lesions when compared with MIBG or FDG-PET. The limitations of DWI were possible false-positive finding, and probable lower detectability of mediastinal lymph node and lung metastasis.

Keywords Diffusion-weighted magnetic resonance imaging (DWI-MRI) · 2-[^{18}F]-fluoro-2-deoxy-D-glucose positron emission tomography (^{18}F-FDG PET) · ^{123}I-meta-iodo-benzyl guanidine (^{123}I-MIBG) · Pheochromocytoma · Paraganglioma

Introduction

Pheochromocytoma/paraganglioma is a unique disease that originates from chromaffin cells such as the adrenal medulla and sympathetic ganglia [1]. Malignant pheochromocytoma/paraganglioma is uncommon, and metastases typically affect the bones, liver, lungs, and lymph nodes. There is no reliable non-invasive marker to indicate malignant behavior of pheochromocytoma/paraganglioma, and the only criterion for malignancy appears to be the presence of chromaffin tissue at distant metastasis where chromaffin tissue is normally absent. Paragangliomas of the extra-adrenal sympathetic

A. Takano (✉) · N. Oriuchi · Y. Tsushima · A. Taketomi-Takahashi · T. Nakajima · Y. Arisaka · T. Higuchi · M. Amanuma · K. Endo
Department of Diagnostic Radiology and Nuclear Medicine, Gunma University Graduate School of Medicine, 3-39-22 Showa-machi, Maebashi 371-8511, Japan
e-mail: akie_731014@yhoo.co.jp

nervous system metastasize more often than adrenal pheochromocytoma [2]. The early determination of metastatic lesions is crucial for the long-term prognosis of patients, as it provides opportunity for medical and surgical treatment.

Meta-iodo-benzyl guanidine (MIBG) is a norepinephrine analog, and ^{131}I- and ^{123}I-MIBG have been widely used for the diagnosis of pheochromocytoma/paraganglioma. This technique has high specificity and detectability not only for primary tumors but also metastatic lesions when compared with morphologic imaging such as computed tomography (CT) and magnetic resonance imaging (MRI) [3, 4], but it may show false-negative results in some cases of metastatic pheochromocytoma/paraganglioma because of tumor dedifferentiation, which may result in the loss of norarenergic transportation [4, 5]. Positron emission tomography with 2-[^{18}F]-fluoro-2-deoxy-D-glucose (FDG-PET) has been used for the imaging of various neoplasms including adrenal tumor [6, 7]. FDG-PET may also be useful for staging and assessing therapeutic response of malignant pheochromocytoma/paraganglioma [8, 9], and this technique may depict some metastases which fail to accumulate MIBG [10]. A recent study using FDG-PET, ^{18}F-fluorodopamine PET, MIBG, ^{111}In-pentetreotode, ^{99m}Tc-methylene diphosphate scintigraphy indicated that FDG-PET was the preferable functional imaging modality for the localization of metastatic paraganglioma [11].

Recently, it has been reported that diffusion-weighted MRI (DWI) with high *b*-value has high sensitivity in depicting malignant diseases [12, 13], and whole-body DWI has been proposed as a powerful screening tool. To the best of our knowledge, however, there has been no published study that applied DWI to malignant pheochromocytoma/paraganglioma.

The aim of this study is to investigate the diagnostic features of DWI as compared with FDG-PET and MIBG for metastatic diseases in patients with malignant pheochromocytoma/paraganglioma.

Materials and methods

Patients

We prospectively studied 11 patients [39.9 ± 13.8 years, mean ± standard deviation (SD); range 22–63; six men) with histologically confirmed pheochromocytoma or paraganglioma. Our institutional review board approved the protocol, and each patient gave written informed consent before participating in the study. All patients were referred to the hospital for assessment of the indication of treatment with ^{131}I-MIBG because metastatic disease was highly suspected by imaging modalities such as CT or MRI. Patients who were pregnant, breast feeding, expected to survive less than 1 month, had myelosuppression of hemoglobin <9.0 g/dl or white blood cell count <3000 mm^{-3} or platelet count <100 000 mm^{-3}, or had renal dysfunction equivalent to glomerular filtration rate <30 ml/min were excluded from the study. None of the patients were prescribed drugs known to interfere with the uptake of catecholamines. In all patients, all DWI, FDG-PET, and MIBG examinations were completed within 1 week.

MIBG and FDG-PET examination

^{18}F-FDG was produced in the cyclotron facility of our institute and FDG-PET was performed as described earlier [14]. The patients fasted for at least 6 h before the studies. Imaging was performed using a whole-body PET scanner (SET 2400 W; Shimadzu, Kyoto, Japan) with 59.5 cm transverse fields of view and 20-cm long, which produced 63 image planes with a 3.123-mm interval between images. Transverse resolution at the center of the field of view was 4.2 mm in full width half maximum. Two-dimensional data acquisition was initiated 50 min after the injection of 5 MBq/kg of ^{18}F-FDG. The image protocol was set to use a simultaneous emission–transmission method with a rotating external source using ^{68}Ge and to acquire 4 to 8 bed positions (8 min acquisition per bed position) according to the range of imaging. Attenuation-corrected transverse images were reconstructed with the ordered-subsets expectation maximization algorithm into 128 · 128 matrix with pixel dimensions of 4.0 mm in plane and 3.125 mm axially. Coronal images with a 9.8-mm section thickness were also reconstructed from attenuation-corrected transverse images for visual interpretation.

Following intravenous injection of 222 MBq ^{123}I-MIBG, whole-body imaging was performed in anterior and posterior projections at 6 h and 24 h after administration. Planar scintigraphy was acquired with a dual-head gamma-camera (E-CAM, Siemens, Munich, Germany) equipped with a medium-energy parallel-hole collimator.

Two experienced nuclear physicians independently interpreted MIBG and FDG-PET images blinded to the results of other imaging modalities, and the final diagnoses were based on a consensus of the two observers. By subjective visual assessment, abnormal positive uptakes on MIBG or FDG-PET images excluding normal physiological uptake were considered to be metastatic lesions.

DWI

Magnetic resonance imaging was performed with a 1.5-T MR system (Symphony/Quantum gradient, Siemens), using a phase-array coil. In addition to conventional T1-weighted gradient echo and T2-weighted fast spin echo images, whole-body (neck through pelvis) axial DWIs were obtained by single-shot spin-echo type echo-planar imaging sequence with inversion pulse (TR/TE = 8000/72, *b*-factor = 1000 s/mm^2, FOV = 400 mm, 128 · 128 matrix, 4 mm slice thickness, gap 0). From these 60 axial DWIs, coronal maximum intensity projection (MIP) images were also created.

Images were interpreted by two radiologists who blinded to the results of other imaging modalities, and the final diagnoses were based on a consensus of the two observers. Abnormal high signal intensities on DWI larger than 5 mm in diameter were interpreted as metastases unless the conventional T1- and T2-weighted images suggested benign lesions.

Results

The characteristics of patients are summarized in Table 1. Nine patients had undergone surgical removal of the primary tumor 2–13 years earlier, and in two other patients, the diagnosis was confirmed by biopsy. FDG-PET and DWI demonstrated metastatic lesions in all 11 patients, but MIBG showed no metastatic lesions in 2 patients. Bone metastasis was most commonly seen (82%; 9 of 11 patients), followed by lymph node and liver metastasis (36%, respectively; Tables 1, 2; Fig. 1).

A total of 130 foci were detected by DWI, FDG-PET, or MIBG. Either PET or MIBG detected 102 foci. Of these foci, DWI, PET, and MIBG detected 91 foci

Table 1 Patient characteristics

Patient	Age/sex	Primary lesion	Metastasis			
			Lymph node	Bone	Liver	Lung
1	22/M	Adrenal gland	+	+		+
2	23/F	Adrenal gland		+		
3	41/M	Adrenal gland	+			
4	51/M	Adrenal gland		+		
5	59/M	Adrenal gland		+		
6	63/F	Adrenal gland	+		+	
7	31/M	Carotid body		+	+	
8	44/F	Carotid body		+	+	
9	36/F	Retroperitoneum		+		
10	45/F	Retroperitoneum	+	+	+	+
11	42/M	Rib		+		

+, Metastasis depicted by 2-[^{18}F]-fluoro-2-deoxy-D-glucose positron emission tomography (FDG-PET), ^{123}I-meta-iodo-benzyl guanidine scintigraphy (MIBG), or diffusion-weighted MR imaging (DWI)

Table 2 Number of metastatic lesions depicted by each imaging modality in the lymph nodes, bone, liver, and lung

Patient	Lymph node metastasis			Bone metastasis			Liver metastasis			Lung metastasis		
	FDG-PET	MIBG	DWI	FDG-PET	MIBG	DWI	FDG-PET	MIBG	DWI	FDG-PET	MIBG	DWI
Pheochromocytoma												
1	1	2	0*	2	6	5	0	0	0	1**	4	1**
2	0	0	0	1	1	3	0	0	0	0	0	0
3***	8	0	20	0	0	0	0	0	0	0	0	0
4	0	0	0	12	13	10	0	0	0	0	0	0
5	0	0	0	10	15	20	0	0	0	0	0	0
6	3	2	12	0	0	0	0	4	5	0	0	0
Paraganglioma												
7	0	0	0	5	5	5	2	2	2	0	0	0
8***	0	0	0	6	0	6	4	0	5	0	0	0
9	0	0	0	8	7	5	0	0	0	0	0	0
10	7	2	7	4	0	4	3	3	3	4	3	4
11	0	0	0	2	2	2	0	0	0	0	0	0
Total	19	6	39	50	49	60	9	9	15	5	7	5

* Two lymph node metastases in the mediastinum were not depicted on DWI

** Three lung metastases which were positive on MIBG were not depicted on DWI or FDG-PET

*** In two patients, no metastatic lesions were depicted on MIBG

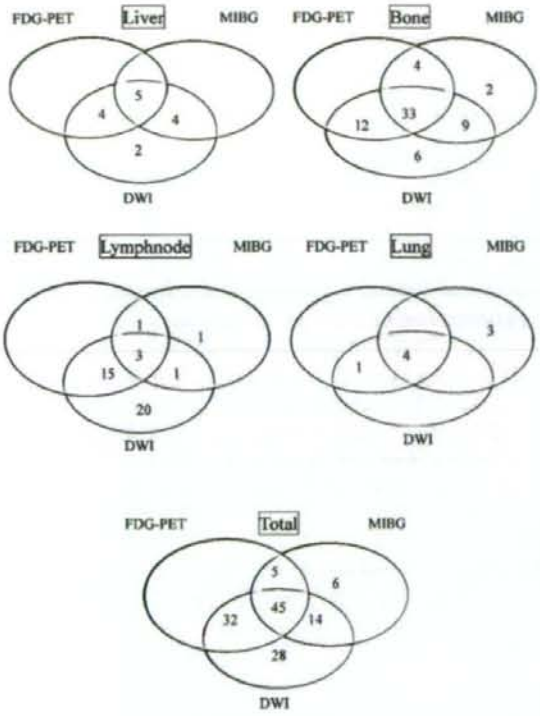

Fig. 1 Number of metastatic lesions depicted by 2-[^{18}F]-fluoro-2-deoxy-D-glucose positron emission tomography (FDG-PET), ^{123}I-meta-iodo-benzyl guanidine scintigraphy (MIBG), and diffusion-weighted magnetic resonance imaging (DWI)

(89.2%), 82 foci (80.3%), and 70 foci (68.6%), respectively. Six foci were detected only with MIBG.

Lymph node metastasis

DWI demonstrated 39 lymph node metastases followed by 19 on FDG-PET, and MIBG depicted only six lymph node metastases. In patient nos. 3 and 6, DWI depicted 20 and 12 lymph nodes, respectively. On the other hand, FDG-PET and MIBG depicted 8 and 3, 0 and 2 lymph nodes, respectively. Most both FDG-PET and MIBG negative foci were less than 1 cm. DWI failed to depict two lymph node metastases in the mediastinum that were clearly demonstrated by MIBG.

Bone metastasis

DWI demonstrated 60 bone metastases, followed by FDG-PET and MIBG. However, four bone metastases, which were demonstrated on FDG-PET, and six, which were seen on MIBG were not demonstrated on DWI.

Liver metastasis

DWI demonstrated 15 liver metastases. FDG-PET failed to show six of them, and MIBG also failed to show six of them. There were no liver metastases, which were seen on FDG-PET or MIBG, but DWI failed to show.

Lung metastasis

MIBG showed seven lung metastases, but three of them were not demonstrated on DWI. These lung metastases were located in the lower lobes.

DWI could detect most of the lesions. DWI failed to detect 11 lesions (six in the bone, three in the lung, and two in the lymph node) in three patients. In two patients (nos. 4 and 9), three and two bone lesions could not be detected, respectively. In patient no. 1, three, two, and one lesion in the lung, lymph node, and bone could not be detected, respectively. Of these lesions, PET could detect four bone lesions (patient nos. 4 and 9) and a lymph node lesion (patient no. 1), whereas MIBG could detect three lung lesions (patient no. 1), six bone lesions (patient nos. 1, 4, and 9), and two lymph node lesions (patient no. 1). Six of these 11 lesions were detected with MIBG alone. In contrast, no lesion was detected with PET alone. Twenty-eight lesions were detected with DWI alone. They included 20 in the lymph node, 6 in the liver and 2 in the bone.

Comparison of PET with MIBG showed that 48 lesions were identified both by PET and MIBG, 32 by PET alone, and 20 by MIBG alone. PET could detect more lesions in the lymph node as compared with MIBG. MIBG could detect more lesions in the lungs as compared with PET. Detectability of PET and MIBG was similar for liver and bone lesions.

Discussion

Although MIBG has been primarily used for the diagnosis of pheochromocytoma/paraganglioma and their metastases, it was notable that only a small number of lymph node metastases were demonstrated on MIBG. In addition, the number of lymph node metastases demonstrated on DWI was more than twice that of FDG-PET (Fig. 2). However, multiple sites of high intensity detected by DWI alone were indeterminate regardless of whether they were normal or abnormal. There were no liver metastases, which were seen on FDG-PET or MIBG but not on DWI. Regarding bone and lung metastases, FDG-PET and DWI revealed very similar results. These results indicate that DWI may have a higher sensitivity as compared with FDG-PET and MIBG, and may be a suitable

imaging method for screening of metastatic disease in patients with malignant pheochromocytoma/paraganglioma. However, considering the fact that normal lymph nodes were visualized in patients and also in healthy controls, specificity of DWI in the detection of lesions, especially of lymph node metastasis may be low.

The mechanism of high signal intensity on DWI is different from those of increased uptake of MIBG and FDG; a high intensity area in DWI indicates a restriction of the diffusion of water molecules in tissue, possibly owing to increased cellularity. Since many normal structures such as the central nervous system, adrenal glands, and sometimes red bone marrow may show high-signal intensity on DWI, body DWI should be always compared with conventional T1- and T2-weighted images [15]. However, false-positive foci could not be excluded, because MRI is not specific for malignant tumor.

We suppose that the low background signal of the liver on high *b*-factor DWI enables depiction of a larger number of liver metastases when compared with MIBG and FDG-PET. A preliminary study comparing DWI with ^{18}F-FDG PET/CT revealed that DWI might be useful in detecting malignant tumors, but it would have been difficult to differentiate between benign and malignant lesions, even though had semiquantitative measurements with an apparent diffusion coefficient been used [16]. In the present study, we evaluated images qualitatively because we did not expect the quantitative value of DWI to detect metastatic lesions.

It should be noted that two lymph node metastases in the mediastinum and three lung metastases in the lower lobes were not demonstrated on DWI. A focus in the lateral segment of the liver was not clear on DWI as shown in Fig. 3. We suppose that physiological motion may degrade the image quality of DWI. Detection of pulmonary and hepatic lesions close to the diaphragm and heart may be limited with DWI.

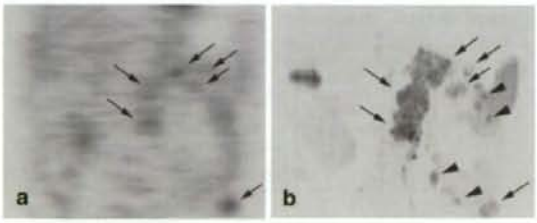

Fig. 2 A 41-year-old man (pt. no. 3) with pheochromocytoma with multiple lymph node metastases. **a** A coronal view of FDG-PET showing multiple foci of FDG uptake in the abdomen (*arrows*). **b** A coronal view of DWI showing multiple foci of high signal intensity in the abdomen corresponding to the FDG-PET (*arrows*). Multiple small foci of high signal intensity were also seen (*arrowheads*). A high intensity in the liver was a biloma due to the operation

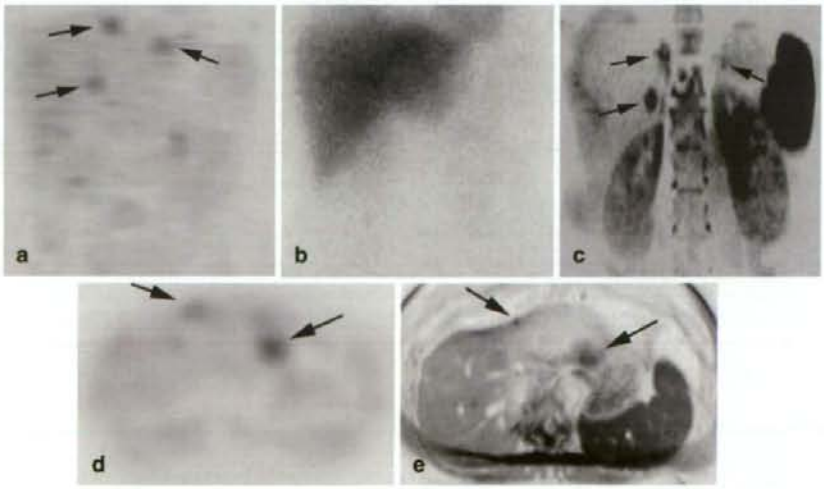

Fig. 3 A 44-year-old woman (pt. no. 8) with carotid body paraganglioma with multiple bone and liver metastases. **a** A coronal view of FDG-PET showing multiple foci of FDG uptake in the liver (*arrows*). **b** Anterior planar image of MIBG failed to show the metastatic lesions seen on FDG-PET in the liver and bone. **c** A coronal view of DWI showing multiple foci of high signal intensity in the liver (*arrows*). The spleen, kidneys, and nerve roots are visualized with very high intensity. **d** An axial view of FDG-PET showing two foci of high FDG uptake in the liver (*arrows*). **e** An axial view of DWI showing multiple foci of high signal intensity in the liver (*arrows*). The intensity of the lesion in the lateral segment was lower as compared with the intensity of the lesion in the medial segment

A comparison between PET and MIBG disclosed that the sensitivity of PET was higher. However, six foci were detected by MIBG and not the other two modalities. In contrast, no lesion was detected by PET and undetected by the other two modalities. Discrepant results of PET and MIBG may be owing to differences in the mechanism of uptake between the two tracers. Uptake of ^{123}I-MIBG and ^{18}F-FDG correlates with sympathetic differentiation and to cellular proliferation and metabolism, respectively. MIBG was superior to PET in detecting lung lesions. This may be because of the lower background activity in the lung and higher lesion-to-background ratio as compared with PET. PET could have possibly detected more foci in the lung and liver had delayed imaging at 2 h been performed. The comparison of PET with MIBG in detecting lymph node metastasis revealed that PET was better than MIBG. This must be partly because of the better spatial resolution and tomographic feature of PET as compared with the planar images of MIBG.

In the present study, ^{123}I-MIBG was used for imaging. Scintigraphy with ^{123}I-MIBG is not widely used in the routine clinical setting. The sensitivity for detecting metastatic lesions is higher with ^{123}I-MIBG than with ^{131}I-MIBG, because of the higher administered dose and better imaging characteristics of ^{123}I. MIBG is highly specific to neuroendocrine tumors and has a key role in deciding internal radiotherapy with ^{131}I-MIBG. As the uptake of MIBG correlates with sympathetic differentiation, de-differentiated lesion, which may be particularly seen in metastatic lesions, may not show increased uptake. A recent study has reported that FDG-PET was useful in defining the distribution of lesions that failed to concentrate ^{123}I-MIBG [8].

There were several limitations in the study. First, the metastatic lesions lacked pathological confirmation. Given that two experienced nuclear physicians interpreted the FDG-PET and MIBG images, it was less likely that benign conditions were misinterpreted as being malignant in patients included in the present study. Twenty-eight foci in five patients were detected by only DWI. These foci were not histologically examined. Clinical follow-up of these five patients including four patients who underwent ^{131}I-MIBG therapy has not confirmed the existence of metastasis in these foci, probably owing to their slow-growing nature and poor response to the therapy. Further clinical follow-up could possibly clarify the specificity of DWI regarding the detection of metastases. High-signal intensity on DWI is not specific for malignant diseases, and a non-specific high signal may sometimes be present, resulting in false-positive results. Second, only patients with suspected inoperable distant metastasis were included in this study, and the number of patients studied was relatively small. Third, the results could not be applied to other malignant tumors.

In conclusion, the results of the current study suggested that DWI might be the most sensitive imaging method for detecting metastatic disease in patients with malignant pheochromocytoma/paraganglioma, rather than MIBG and FDG-PET. However, there was a possibility that the high detectability of DWI results in a high rate of false-positive findings. The comparison between PET and MIBG revealed that PET had better detectability for lymph node metastasis, whereas MIBG could be valuable in detecting bone and lung metastases.

References

1. Lenders JW, Eisenhofer G, Mannelli M, Pacak K. Phaeochromocytoma. Lancet 2005;366:665–75.
2. Edström Elder E, Hjelm Skog AL, Höög A, Hamberger B. The management of benign and malignant pheochromocytoma and abdominal paraganglioma. Eur J Surg Oncol 2003;29:278–83.
3. Lynn MD, Shapiro B, Sisson JC, Beierwaltes WH, Meyers LJ, Ackerman R, et al. Pheochromocytoma and the normal adrenal medulla: improved visualization with I-123 MIBG scintigraphy. Radiology 1985;155:789–92.
4. van der Harst E, de Herder WW, Bruining HA, Bonjer HJ, de Krijger RR, Lamberts SW, et al. [^{123}I] metaiodobenzylguanidine and [^{111}In] octreotide uptake in benign and malignant pheochromocytomas. J Clin Endocrinol Metab 2001;86:685–93.
5. Kaltsas G, Korbonits M, Heintz E, Mukherjee JJ, Jenkins PJ, Chew SL, et al. Comparison of somatostatin analog and metaiodobenzylguanidine radionuclides in the diagnosis and localization of advanced neuroendocrine tumors. J Clin Endocrinol Metab 2001;86:895–902.
6. Oriuchi N, Higuchi T, Ishikita T, Miyakubo M, Hanaoka H, Iida Y, et al. Present role and future prospect of positron emission tomography in clinical oncology. Cancer Sci 2006;97:1291–7.
7. Shimizu A, Oriuchi N, Tsushima Y, Higuchi T, Aoki J, Endo K. High [^{18}F] 2-fluoro-2-deoxy-D-glucose (FDG) uptake of adrenocortical adenoma showing subclinical Cushing's syndrome. Ann Nucl Med 2003;17:403–6.
8. Shulkin BL, Thompson NW, Shapiro B, Francis IR, Sisson JC. Pheochromocytomas: imaging with 2-[fluorine-18] fluoro-2-deoxy-D-glucose PET. Radiology 1999;212:35–41.
9. Menzel C, Graichen S, Berner U, Risse JH, Diehl M, Dbert N, et al. Monitoring the efficacy of iodine-131-MIBG therapy using fluorine-18-FDG-PET. Acta Med Austriaca 2003;30:37–40.
10. Ezuddin S, Fragkaki C. MIBG and FDG PET findings in a patient with malignant pheochromocytoma: a significant discrepancy. Clin Nucl Med 2005;30:579–81.
11. Timmers HJLM, Kozupa A, Chen CC, Carrasquillo JA, Ling A, Eisenhofer G, et al. Superiority of fluorodeoxyglucose positron emission tomography to other functional imaging techniques in the evaluation of metastatic *SDHB*-associated pheochromocytoma and paraganglioma. J Clin Oncol 2007;25:2262–9.

12. Takahara T, Imai Y, Yamashita T, Yasuda S, Nasu S, van Cauteren M. Diffusion weighted whole body imaging with background body signal suppression (DWIBS): technical improvement using free breathing, STIR and high resolution 3D display. Radiat Med 2004;22:275–82.
13. Koh DM, Collins DJ. Diffusion-weighted MRI in the body: applications and challenges in oncology. AJR Am J Roentgenol 2007;188:1622–35.
14. Iwata R, Ido T, Takahashi T, Monma M. Automated synthesis system for production of 2-deoxy-2-[^{18}F] fluoro-D-glucose with computer control. Int J Appl Radiat Isot 1984;35: 445–54.
15. Tsushima Y, Takano A, Taketomi-Takahashi A, Endo K. Body diffusion-weighted MR imaging using high b-value for malignant tumor screening: usefulness and necessity of referring to T2-weighted images and creating fusion images. Acad Radiol 2007;14:643–50.
16. Komori T, Narabayashi I, Matsumura K, Matsuki M, Akagi H, Ogura Y, et al. 2-[^{18}F]-fluoro-2-deoxy-D-glucose positron emission tomography/computed tomography versus whole-body diffusion-weighted MRI for detection of malignant lesions: initial experience. Ann Nucl Med 2007;21:209–15.

Prognostic implication of *SYT-SSX* fusion type in synovial sarcoma: A multi-institutional retrospective analysis in Japan

SATOSHI TAKENAKA[1,2], TAKAFUMI UEDA[3], NORIFUMI NAKA[2], NOBUHITO ARAKI[2], NOBUYUKI HASHIMOTO[1], AKIRA MYOUI[1,4], TOSHIFUMI OZAKI[5], TOMITAKA NAKAYAMA[6], JUNYA TOGUCHIDA[6,7], KAZUHIRO TANAKA[8], YUKIHIDE IWAMOTO[8], AKIHIKO MATSUMINE[9], ATSUMASA UCHIDA[9], MAKOTO IEGUCHI[10], MITSUNORI KAYA[11], TAKURO WADA[11], ICHIRO BABA[12], IKUO KUDAWARA[3], YASUAKI AOKI[13] and HIDEKI YOSHIKAWA[1]

[1]Department of Orthopaedics, Osaka University Graduate School of Medicine, Suita; [2]Department of Orthopaedic Surgery, Osaka Medical Center for Cancer and Cardiovascular Diseases, Osaka; [3]Department of Orthopaedic Surgery, Osaka National Hospital, Kinki-Block Comprehensive Cancer Center, Osaka; [4]Medical Center for Translational Research, Osaka University Hospital, Suita; [5]Department of Orthopaedic Surgery, Okayama University Graduate School of Medicine, Dentistry and Pharmaceutical Sciences, Okayama; [6]Department of Orthopaedic Surgery, Kyoto University Graduate School of Medicine, Kyoto; [7]Department of Tissue Regeneration, Institute for Frontier Medical Sciences, Kyoto University, Kyoto; [8]Department of Orthopaedic Surgery, Graduate School of Medical Sciences, Kyushu University, Fukuoka; [9]Department of Orthopaedic Surgery, Mie University Postgraduate School of Medicine, Tsu; [10]Department of Orthopaedic Surgery, Osaka City University Graduate School of Medicine, Osaka; [11]Department of Orthopaedic Surgery, Sapporo Medical University School of Medicine, Sapporo; [12]Department of Orthopaedic Surgery, Osaka Medical College, Takatsuki; [13]Department of Orthopaedic Surgery, Himeji Red Cross Hospital, Himeji, Japan

Received September 28, 2007; Accepted November 2, 2007

Abstract. The prognostic implication of *SYT-SSX* fusion type in synovial sarcomas is still controversial. The aim of this study is to clarify the prognostic impact of fusion type, in association with other clinical factors, in patients with synovial sarcoma in Japan. Data on 108 *SYT-SSX* fusion transcript-positive patients with synovial sarcoma, treated in 11 tertiary referral cancer centers in Japan, were retrospectively analyzed. The following parameters were examined for their potential prognostic impact: *SYT-SSX* fusion type, patient age at presentation, sex, primary tumor location, tumor size, histological subtype, histological grade, treatment modalities and disease stage at presentation. Among the patients with localized disease at presentation, 5-year overall survival (OS) for *SYT-SSX1* and *-2* subgroups were 84.4 and 74.9%, respectively (P=0.244). Five-year metastasis-free survival (MFS) rates were 67.8% for *SYT-SSX1* and 68.5% for *SYT-SSX2* (P=0.949). Univariate survival analyses for 91 patients with localized disease at presentation showed that tumor size was the only significant prognostic factor for OS (P=0.0033) and MFS (P=0.0029) and the histological grade was marginally significant for MFS (P=0.0785), whereas the *SYT-SSX* fusion type and other variables were not. Multivariate survival analyses further indicated that tumor size was the most significant independent prognostic factor for OS and MFS and the histological grade was also significant for MFS. In conclusion, the *SYT-SSX* fusion type is not a significant prognostic factor unlike tumor size, followed by histological grade for patients with localized synovial sarcoma in Japan.

Correspondence to: Dr Takafumi Ueda, Department of Orthopaedic Surgery, Osaka National Hospital, Kinki-Block Comprehensive Cancer Center, 2-1-14 Hoenzaka, Chuo-ku, Osaka 540-0006, Japan
E-mail: uedat@onh.go.jp

Key words: synovial sarcoma, fusion gene, prognostic factor, *SYT-SSX*

Introduction

Synovial sarcoma is a relatively aggressive soft-tissue sarcoma that accounts for 5 to 10% of all soft-tissue sarcomas and mainly affects adolescents and young adults (1). Synovial sarcomas are histologically divided into three subtypes: a biphasic subtype containing both epithelial and spindle tumor cells, a monophasic subtype composed solely of spindle tumor cells and a poorly differentiated subtype composed of primitive oval or short-spindle-shaped tumor cells (2). Cytogenetically, however, >95% of synovial sarcomas bear the translocation t(X;18)(p11.2;q11.2), which is a chromosomal re-arrangement specific to this tumor (3). The translocation represents the fusion of the *SYT* gene on the 18q11.2 chromosome with the

SSX1 or -2 gene, both of which are closely located on chromosome Xp11.2. The precise function of this chimeric gene still remains unknown, though it has recently been used as a specific diagnostic marker for this tumor (4).

As well as its diagnostic significance, the fusion type has recently been proposed to be a prognostic factor. Kawai *et al* (5) and subsequently Ladanyi *et al* (6) reported that the *SYT-SSX1* form of synovial sarcoma, compared to that of *SYT-SSX2*, has a significantly unfavorable prognosis. Thereafter, several reports with a relatively small number of case series have supported the positive prognostic implication of *SYT-SSX* fusion type in patients with synovial sarcoma (7-9). In contrast, Guillou *et al* most recently showed a trend for tumors bearing *SYT-SSX2* transcripts to behave more aggressively than those of *SYT-SSX1*, but the difference was not statistically significant (10). Thus, the prognostic implication of the *SYT-SSX* fusion type in synovial sarcomas is still controversial. To address this issue, we conducted the present study to investigate the prognostic impact of the fusion type, in association with other clinical factors, in patients with synovial sarcoma in Japan.

Patients and methods

As a multi-institutional retrospective study, 108 patients with SYT-SSX-positive synovial sarcoma treated in 11 tertiary referral cancer centers or university hospitals in Japan from 1978 to 2005 were enrolled. All patients were histologically diagnosed as having synovial sarcoma on routine hematoxylin and eosin stains with appropriate immunohistochemical examinations, including a set of epithelial markers such as cytokeratins and epithelial membrane antigen (EMA) in each center, and were confirmed with the detection of *SYT-SSX* fusion transcripts using the RT-PCR method in frozen tumor samples. We have retrospectively collected patient data from their clinical records including the data on the *SYT-SSX* fusion type, patient age at presentation, sex, primary tumor location, tumor size, histological subtype, histological grade, treatment modalities and disease stage (presence or absence of metastasis) at presentation. Extremity tumors were defined as tumors located in free extremities only, but extremity girdles including the shoulder, axilla, groin or buttock were considered to be trunk locations. Tumor size was defined as the maximum dimension on a magnetic resonance imaging (MRI) or computed tomography (CT) scan. Histological subtyping was carried out on routine hematoxylin and eosin stains using the 2002 WHO classification of tumors (11). Histological grading was based on the criteria of Enzinger and Weiss and assigned to three grades (1, 2 and 3), using several essential histopathological parameters such as cellularity, mitotic activity, tumor necrosis, with or without Ki-67 reactivity as a reliable cell proliferation index (12-16). All patients were treated by the multimodality therapeutic approach, combined with surgery, chemotherapy and/or radiotherapy. Wide local excision for the primary tumors was generally attempted as much as complete re-section was considered possible. Consequently, 63 out of 108 patients underwent wide local excision, 13 patients received marginal excision, 9 intralesional excision, 4 local tumor re-section with an undetermined surgical margin and 15 amputation of the affected limb. The other 4 patients with metastatic disease did not undergo definitive surgery for the primary tumors. Chemotherapy was performed in 83 out of 108 patients (76.9%), 68 of whom had localized disease and 15 metastatic disease at presentation. The regimens of chemotherapy varied in each center, but mainly included ifosfamide and/or doxorubicin with the exception of 3 cases. Radiotherapy was performed in 23 patients (21.3%) pre- and/or postoperatively with a mean dose of 43.8 Gy (range: 28-70 Gy). The decision to give adjuvant therapy (chemotherapy and/or radiotherapy) was made independently by each center.

Fusion type analysis. The frozen tumor samples were mostly obtained from the primary site (79 cases), but in some cases from locally recurrent (14 cases) or metastatic sites (3 cases). The other 12 samples were obtained from unspecified tumor sites. Almost all patients were analyzed for the *SYT-SSX* fusion type by reverse transcription-polymerase chain reaction (RT-PCR) using the *SYT* primer: 5'-caacagcaagatgcatacca-3', the *SSX1* specific primers: 5'-ggtgcagttgtttcccatcg-3' and the *SSX2* specific primers: 5'-ggcacagctctttcccatca-3' in most cases, but in some cases using the SSX common primer: 5'-cacttgct atgcacctgatg-3', followed by direct sequencing.

Statistical analysis. For statistical analysis, the following variables were potentially considered for their prognostic factors: patient age at presentation, sex, primary tumor location, tumor size, histological subtype, histological grade, treatment modalities, disease stage at presentation and fusion type. The correlations between these factors were analyzed using the Pearson χ^2 test. Overall survival (OS) was defined as the time from the beginning of treatment to the death of the patient. Metastasis-free survival (MFS) was defined as the first metastasis interval from the beginning of treatment. Patients who died from unrelated causes to sarcoma were censored at the time of death. OS and MFS curves were computed by the Kaplan and Meier method (17). We compared these curves by using the log-rank test (18) for univariate survival analysis. Two-tailed P-values of ≤ 0.05 were estimated as statistically significant for the prognostic factors. Cox's proportional hazards model was used to identify independent factors predictive of survival for multivariate analysis (19). Patient age at presentation was also evaluated as a continuous variable by Cox's regression model. These statistical analyses were performed using the JMP version 5.01 statistical analysis software package for personal computers (SAS Institute Inc, Cary, NC, USA).

Results

Patient and tumor characteristics. The patient and tumor characteristics are summarized in Table I. *SYT-SSX1* and -2 fusion transcripts were detected in 68 (63.0%) and 40 (37.0%) cases, respectively. There were 44 men (40.7%) and 64 women. The median age at presentation was 37 (mean, 33 years), ranging from 8 to 74 years. Forty-seven patients (43.5%) were aged ≤30. Seventy-two extremity-based tumors included lower (n=61) and upper extremities (n=11). Thirty-six truncal tumors included lower-extremity (n=17) and upper-extremity girdles (n=5), head and neck (n=2) and abdominal wall (n=12). The data on maximal tumor size were available